Progress In Electromagnetics Research Letters, Vol. 92, 117–124, 2020

Balanced Reconfigurable Filter Using Liquid Metal

Miguel-Antonio Romero-Ramirez[1], Jose Luis Olvera-Cervantes[1], Tejinder Kaur Kataria[2], and Alonso Corona-Chavez[1, *]

Abstract—A novel balanced bandpass reconfigurable microstrip filter is presented, where in differential mode, the filter operates in seven different bands, and each inductor L_M represents a state of frequency. The common mode rejection ration (CMRR) is better than 30 dB for all the states. The central frequency of the filter is changed by liquid metal droplets flowing along a microfluidic channel placed at the middle of the inductors L_M. For demonstration, a third-order filter is designed, simulated, and fabricated, operating in the S-band. Good agreement between simulation and measurement is presented.

1. INTRODUCTION

Research in reconfigurable and tunable balanced bandpass filters has been increasing in the last decades due to their advantages in modern wireless communication systems [1].

One way to design tunable balanced filters is implementing microelectromechanical systems (MEMS) or varactors. Varactors can change the central frequency when they are located at specific places of multi-mode resonators [2] and stepped impedance resonators [3]. Nevertheless, varactors offer nonlinear behavior and high insertion loss. MEMS switches can deal with these problems, but they have reliability issues [4]. Moreover, for several band reconfiguration, several switches may be needed, such as in [5], where a tunable bandpass filter uses 20 MEMS switches, where two switches need to be connected at a time to change the central frequency.

Liquid metal is a new way for designing reconfigurable balanced filters that present low loss, linear behavior, and high-power handling. Galinstan (GaInSn) is a non-toxic liquid metal alloy which has been used for reconfigurability in microwave devices, such as monopole antennas, double-stub tuners, and filters [6, 7]. In [8], a low-pass filter uses liquid metal to reconfigure the cutoff frequency. In [9], a bandpass filter based on split ring resonators is presented where liquid metal is used to reshape the resonators and change the central frequency. Technologies such as coplanar waveguides (CPW) [10] and substrate integrated waveguides (SIW) [11] have been designed with liquid metal to change operation frequencies and responses. In [12], a dual-band band-pass filter with three different states is presented, where the reconfigurability is achieved by changing the stub length with liquid metal. A filter based on dual-mode ring resonators which allows tuning external quality factor and center frequency is presented in [13], and this filter has fourteen liquid metal switches, where it is necessary to connect eight, six, and four switches to change among the three different central frequencies. In [14], a two-pole quarter-wavelength filter is presented containing five plastic tubes above the resonators which are filled with high-permittivity water to change the central frequency. A tunable differential dual-mode patch filter is presented in [15], where eight microfluidic channels are filled with distilled water in four different combinations to reconfigure the central frequency.

On the other hand, balanced filters are widely used in modern communications systems due to their high immunity to common mode noise [16]. A few balanced microwave liquid metal reconfigurable filters

Received 23 January 2020, Accepted 10 June 2020, Scheduled 14 July 2020

* Corresponding author: Alonso Corona-Chavez (alonsocorona@inaoep.mx).

[1] National Institute for Astrophysics, Optics and Electronics (INAOE), Puebla, Mexico. [2] Electronics Department, DICIS, University of Guanajuato, Mexico.

can be found in the literature. For example, in [17], a balanced liquid metal reconfigurable microstrip filter based on close loop transmission lines is presented, where the reconfiguration is achieved by liquid metal droplets located at the symmetry plane.

In this letter, a novel balanced bandpass reconfigurable filter in the S-band is presented. It is based on a novel balanced liquid metal reconfigurable resonator composed by transmission lines (TLs) and inductors. The filter works in seven different bands when it is operated in differential mode and in a unique common mode for all bands. The reconfigurable central frequency is achieved by switches placed in the middle of the inductors (L_M). A microfluidic channel is installed in the switches to make the liquid metal droplets flow and fill the switches. Galinstan was chosen because it is liquid at room temperature, and it is nontoxic. The advantage of this work is that a microchannel can be placed along the reconfigurable lines, such that only one liquid metal droplet is used to reconfigure the 7 resonant frequencies by adjusting the pumping pressure, as opposed to conventional technology where several switches are needed, such as in [5, 13–15, 17].

2. PROPOSAL OF THE NOVEL RESONATOR

We begin with the analysis of the balanced reconfigurable resonator. The electric circuit is shown in Fig. 1(a), and it is composed by four TLs loaded with two fixed value inductors L_E and one variable inductor L_M. The two fixed value inductors L_E are always connected and provide inductive coupling between resonators. The variable inductor L_M contains seven inductors L_M located along the transmission lines. Each of these inductors provides a unique resonant frequency, so we have seven different resonance frequencies. The reconfiguration of central frequency is achieved by the L_M inductors located along the transmission lines. A switch is placed in the middle of each of them, and a cylindrical tunnel forming a microfluidic channel is placed along the switches, where a liquid metal droplet fills one switch at a time to reconfigure the resonant frequency. A micropump is used to change the location of the droplet. To make the droplets flow through the switches, NaOH is utilized to encapsulate the liquid metal.

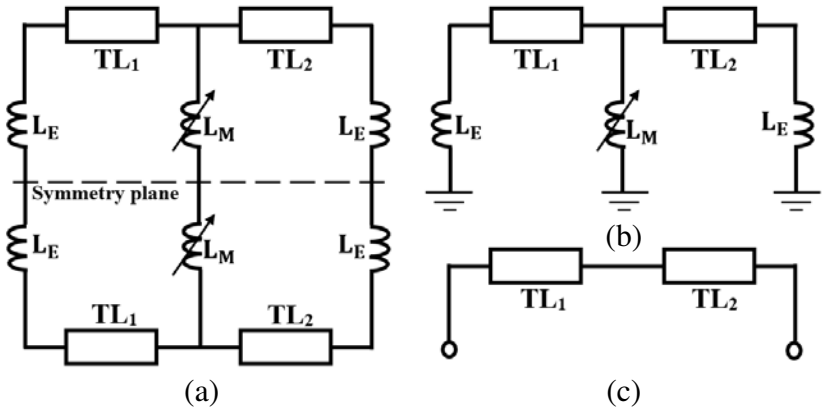

Figure 1. (a) Equivalent circuit of the resonator, (b) differential mode equivalent circuit and (c) common mode equivalent circuit.

A micropump is used to inject liquid metal droplets to different switches that fill the inductor gaps to enable them. In order to move the metal droplets in the opposite direction, the micropump is used by drawing pressure.

2.1. Common Mode Analysis

In common mode, a magnetic wall appears in the symmetry plane, so no current flows through the inductors. For this reason, the equivalent circuit is composed only by TLs terminated in open circuit and connected in series as shown in Fig. 1(c). Each transmission line has an electrical length θ_{TL} and

an impedance Z_{TL}. Assuming a lossless transmission line, the input impedance under common mode is shown in Eq. (1) [18].

$$Z_{in}^{cc} = -jZ_{TL}\cot\theta_{TL} \tag{1}$$

Resonance occurs when the electrical length equals π, so each transmission line in common mode has an electrical length of $\theta_{TL} = \pi/2$ because they are connected in series. The total electrical length equals π. The common mode electrical length as frequency function is shown in Eq. (2).

$$\theta = \theta_{TL}\frac{f}{f_c} \tag{2}$$

2.2. Differential Mode Analysis

Under differential mode, an electric wall appears in the symmetry plane. Therefore, the electric circuit is composed by two TLs loaded with three grounded inductors, as shown in Fig. 1(b). The input admittance of the equivalent circuit under differential mode is shown in Eq. (3). The condition of resonance is achieved when the admittance equals zero; if we defined the L_E values, electrical length θL_T of TLs, impedance Z_{LT} of TLs, differential resonance frequency f_d, and common resonance frequency f_c, we can evaluated L_M with Eq. (4).

$$Y_{in}^{dd} = \frac{1}{jd} - \frac{j\left[\left(Z_{TL} - c\tan\theta\right)(a) + (c)\,(b)\right]}{Z_{TL}\left[\left(Z_{TL}\tan\theta + c\right)(a) + \left(c\tan\theta\right)(b)\right]} \tag{3}$$

$$L_M = \frac{Z_{TL}a}{e\tan\theta - Z_{TL}\omega_d - \dfrac{\left(Z_{TL}\omega_d\tan\theta + e\right)(b)}{a}} \tag{4}$$

where $a = (\omega_d L_E + Z_{TL}\tan\theta)$, $b = (Z_{TL} - \omega_d L_E\tan\theta)$, $c = (\omega_d L_M)$, $d = (\omega_d L_E)$, $e = \omega_d^2 L_E$ and $\omega_d = 2\pi f_d$.

One resonator is designed to work at the S-band, in a frequency range from 2.76 GHz to 3.00 GHz. The Δf between bands is 40 MHz, and the values of the elements of the electrical circuit are: $f_c = 6$ GHz, $\theta_{TL} = \pi/2$, $Z_{TL} = 25\,\Omega$, and $L_E = 2.36$ nH. The values of L_M for each state are listed in Table 1. The layout of the proposed reconfigurable resonator is shown in Fig. 2, where the TLs TL_1 and TL_2 are designed with microstrip lines and connected in series. L_E inductors are designed with high impedance straight lines. Inductor L_{M7} is designed with the same geometry as L_E. The inductor of Fig. 1 is a variable inductor that can be implemented with several topologies such as a chip inductor, a microstrip spiral, or a high impedance microstrip line. For our design, 7 high impedance microstrip lines are placed in parallel (Fig. 1). Inductors L_{M1} to L_{M6} are designed with high impedance meander microstrip lines and connected along the TLs. The simulated resonant frequencies of the resonator are shown in Fig. 3. The dimensions of the resonator of Fig. 2 are: $a = 5.96$ mm, $b = 5.15$ mm, $c = 17.05$ mm, $d = w = 3.5$ mm, $e = 1.63$ mm, $f = h = u = 1.07$ mm, $g = t = 2.50$ mm, $i = r = 1.57$ mm, $j = q = 1.50$ mm, $k = 0.67$ mm, $l = o = 2.07$ mm, $m = 0.3$ mm, $n = 2.42$ mm, $p = 1.15$ mm, $s = 1.52$ mm, $v = 1.21$ mm, $x = 0.25$ mm.

Table 1. Values for the inductors L_M for each state.

State	Resonance (GHz)	Value of L_M (nH)
1	2.76	$L_{M1} = 4.09$
2	2.80	$L_{M2} = 3.67$
3	2.84	$L_{M3} = 3.32$
4	2.88	$L_{M4} = 3.02$
5	2.92	$L_{M5} = 2.77$
6	2.96	$L_{M6} = 2.55$
7	3.00	$L_{M7} = 2.36$

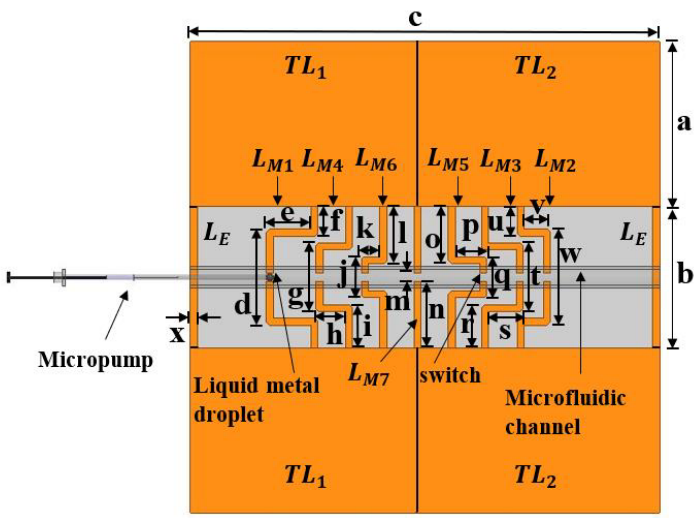

Figure 2. Layout of the proposal resonator indicating dimensions and the microfluidic channel.

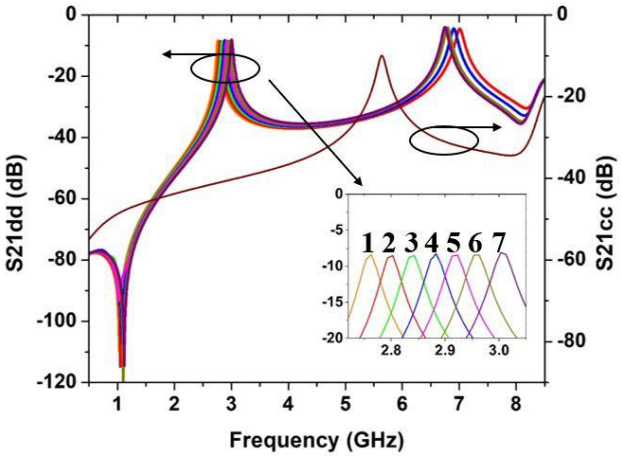

Figure 3. Simulation of the resonator under differential and common mode.

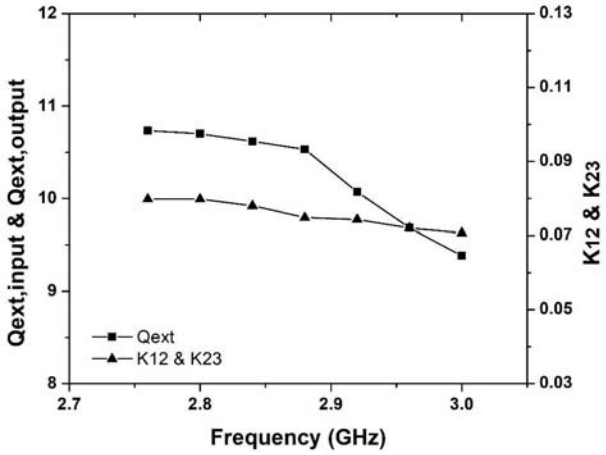

Figure 4. External quality factor ($Q_{\text{ext, input}}$, $Q_{\text{ext, output}}$) and mutual coupling coefficients ($k_{1,2}$ and $k_{2,3}$) versus frequency.

3. DESIGN OF THE BALANCED BANDPASS RECONFIGURABLE FILTER

There are two parameters that define microstrip filter design, which are the input and output external quality factors and the coupling coefficient between resonators, expressed in Equations (5), (6), and (7), respectively [19].

$$Q_{\text{ext, input}} = \frac{g_0 g_1}{\text{FBW}} \tag{5}$$

$$Q_{\text{ext, output}} = \frac{g_n g_{n+1}}{\text{FBW}} \tag{6}$$

$$K_{i,i+1} = \frac{\text{FBW}}{\sqrt{g_i g_{i+1}}} \tag{7}$$

where FBW is the fractional bandwidth, and g parameters are the normalized parameters of the low-pass prototype defined in [19].

Based on the reconfigurable resonator, a three-pole bandpass filter with Butterworth response and FBW = 10% is designed using [16]. The normalized g parameters, input and output external quality factors, and the couplings coefficients for the filter specifications are:

$$\begin{aligned} g_0 &= g_1 = g_3 = g_4 = 1 \quad \text{and} \quad g_2 = 2 \\ Q_{\text{ext, input}} &= Q_{\text{ext, output}} = 10 \\ K_{1,2} &= K_{2,3} = 0.0707 \end{aligned}$$

The substrate has a relative permittivity of $\varepsilon_r = 2.33$ and height of $h = 0.787$ mm. In simulation, the input and output quality factors $Q_{\text{ext, input}}$, $Q_{\text{ext, output}}$ are obtained by connecting a differential port at a distance 2.51 mm from the symmetry plane. The mutual coupling coefficients $K_{1,2}$ and $K_{2,3}$ are achieved by coupling resonators with a separation of 0.3 mm. Fig. 4 shows $Q_{\text{ext, input}}$, $Q_{\text{ext, output}}$ vs f and $K_{1,2}$ and $K_{2,3}$ vs f, which shows a nearly constant behavior in the frequency range.

4. SIMULATION AND EXPERIMENTAL RESULTS

The simulation of the filter is shown in Fig. 5, where seven bands with an FBW from 8.8% to 12.5% are visible. The filter is fabricated with a photolithography process and measured with a two-port network analyzer. To convert the 2 port measurements into mixed port signals, the procedure in [16] is followed. The measurement is shown in Fig. 6. For common mode, the layout is composed by the TLs and half of the inductors. The electrical length of the inductors is 1/6 of the TLs; therefore, these inductors slightly affect the common mode resonance, which is located at 5.36 GHz. Table 2 shows the simulated and measured central frequencies (C.F), measured insertion loss (I.L), return loss (R.L), and the measured FBW for each state. The measured and simulated common mode attenuations for all bands are below 30 dB. The filter has a size of $0.69\lambda \times 0.23\lambda$, where λ is one wavelength calculated on the substrate at 2.88 GHz and at 50 Ω. Fig. 7(a) shows the filter structure composed by three directly coupled reconfigurable resonators without the microfluidic channel: Here, the central inductors L_M can be clearly appreciated. Fig. 7(b) shows the final filter structure. We have installed the microfluidic channel in each resonator with the requirements of Fig. 2.

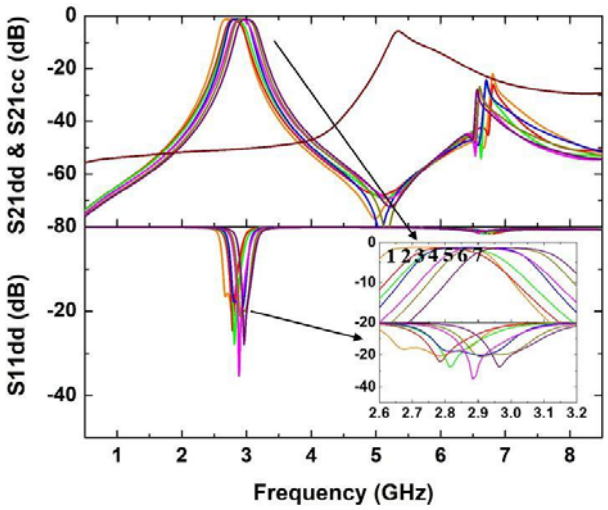

Figure 5. Simulation of the filter under differential and common mode operation.

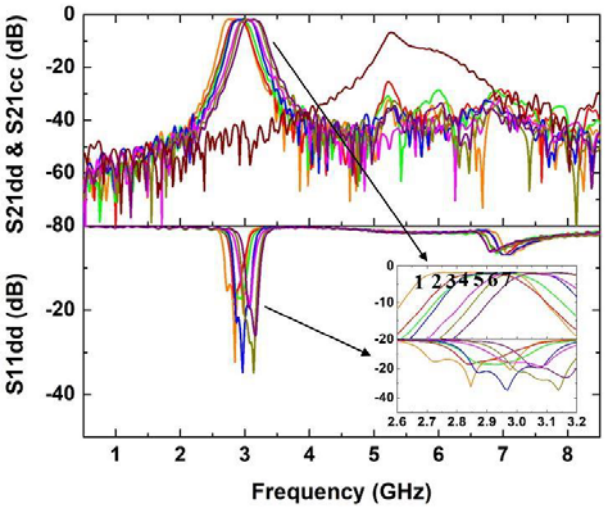

Figure 6. Measurement of the filter under differential and common mode operation.

Figure 8 shows the common mode rejection ratio (CMRR) simulated and measured for state 1, showing a peak value of 40 dB at 2.84 GHz. The values of the other states are better than 30 dB. The CMRR value is obtained from Eq. (8) [20].

$$\text{CMRR} = 20 \log \left(\frac{S_{21}^{dd}}{S_{21}^{cc}} \right) \tag{8}$$

Table 2. Characteristics of the measured filter.

State	C.F Sim.	C.F Meas.	I.L (dB) Meas.	R.L (dB) Meas.	FBW (%) Meas.
1	2.760	2.840	1.67	13.70	13.20
2	2.802	2.890	2.17	17.00	9.10
3	2.840	2.930	2.10	17.00	10.00
4	2.881	2.970	1.78	18.60	12.00
5	2.921	3.020	1.90	16.00	9.70
6	2.960	3.070	1.88	28.00	10.10
7	3.000	3.110	1.85	19.00	9.70

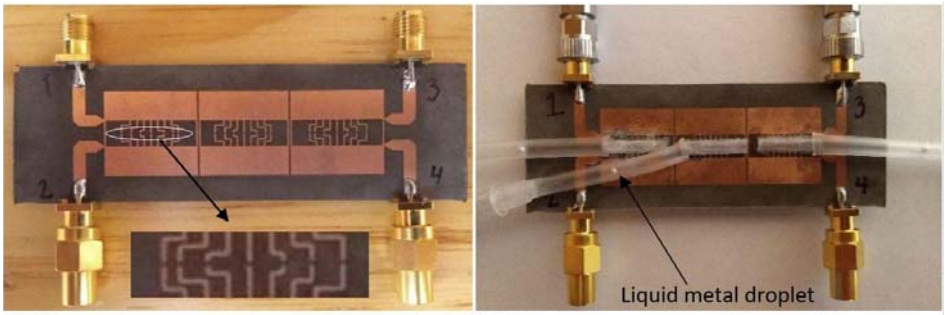

(a) (b)

Figure 7. Fabricated filter (a) before microfluidic channel implementation and (b) after microfluidic channel implementation.

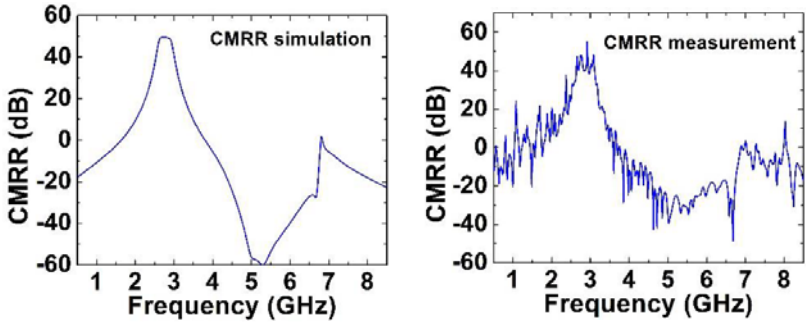

(a) (b)

Figure 8. (a) Simulated CMRR for state 1 and (b) measured CMRR for state 1.

Figure 9 shows the group delay for state 1, showing a maximum value of 3.22 ns at the edge of the passband. The group delay is calculated from Eq. (9) [21]. The other states are near 3 ns at the edge of the passband.

$$\text{Group Delay} = -\frac{d\varphi}{d\omega} \tag{9}$$

Table 3 shows a comparison between previous works related with tunable filters with metal liquid and this work.

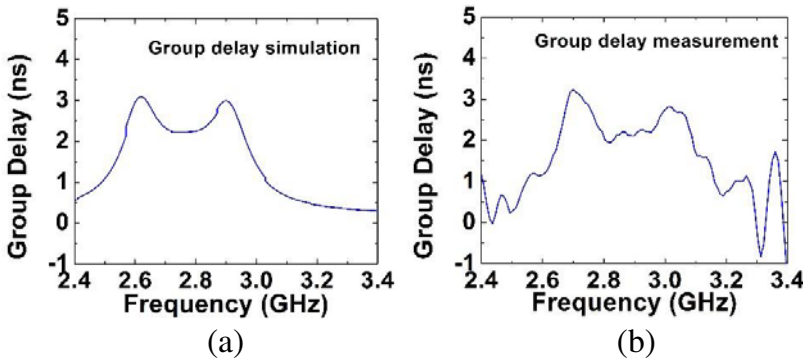

Figure 9. (a) Simulated group delay for state 1 and (b) measured group delay for state 1.

Table 3. Comparison with previous works.

Work	Number of bands	Frequency range (GHz)	Insertion loss (dB)	$\lvert S_{21}^{cc}\rvert$ (dB)	FBW (%)	Technology
[9] 2013	4	0.65–0.87	< 3	no	5	Microstrip
[12] 2017	2	1.85–3.06	2.5–3.21	no	2.71–4.34	Microstrip
[13] 2018	3	0.91–1.75	0.47–0.69	no	15	Microstrip
[17] 2017	2	1.64–2.029	1.6–2	< 30	7.5–10.9	Microstrip
This	7	2.84–3.11	1.67–2.17	< 40	9.1–13.2	Microstrip

5. CONCLUSION

In this work, a novel balanced bandpass microstrip liquid metal reconfigurable filter is presented. It works in a frequency range from 2.84 GHz to 3.11 GHz and shows an attenuation in common mode better than 30 dB in the whole frequency range. The reconfiguration is achieved by liquid metal switches placed at the L_M inductors.

REFERENCES

1. Rais-Zadeh, M., J. T. Fox, D. D. Wentzloff, and Y. B. Gianchandani, "Reconfigurable radios: A possible solution to reduce entry costs in wireless phones," *Proc. IEEE*, Vol. 103, No. 3, 438–451, 2015.
2. Zhang, S. X., Z. H. Chen, and Q. X. Chu, "Compact tunable balanced bandpass filter with novel multi-mode resonator," *IEEE Microw. Wirel. Components Lett.*, Vol. 27, No. 1, 43–45, 2017.
3. Deng, H. W., L. Sun, F. Liu, Y. F. Xue, and T. Xu, "Compact tunable balanced bandpass filter with constant bandwidth based on magnetically coupled resonators," *IEEE Microw. Wirel. Components Lett.*, Vol. 29, No. 4, 264–266, 2019.
4. Rebeiz, G. M., K. Entesari, I. C. Reines, S.-J. Park, M. A. El-Tanani, A. Grichener, and A. R. Brown, "Tuning into RF MEMS," *IEEE Microwave Magazine*, Vol. 10, No. 6, 55–72, Oct. 2009.
5. Amir, S., M. Dousti, and K. Mafinezhad, "A novel analytical technique to design a tunable bandpass filter with constant bandwidth," *International Journal of Electronics and Communications (AEÜ)*, Vol. 70, 1433–1442, 2016.
6. Dang, J. H., R. C. Gough, A. M. Morishita, A. T. Ohta, and W. A. Shiroma, "Liquid-metal-based reconfigurable components for RF front ends," *IEEE Potentials*, Vol. 34, No. 4, 24–30, 2015.

7. Liu, T., P. Sen, and C. J. Kim, "Characterization of nontoxic liquid-metal alloy galinstan for applications in microdevices," *J. Microelectromechanical Syst.*, Vol. 21, No. 2, 443–450, 2012.
8. Guo, S., B. J. Lei, W. Hu, W. A. Shiroma, and A. T. Ohta, "A tunable low-pass filter using a liquid-metal reconfigurable periodic defected ground structure," *IEEE MTT-S Int. Microw. Symp. Dig.*, 1–3, 2012.
9. Mumcu, G., A. Dey, and T. Palomo, "Frequency-agile bandpass filters using liquid metal tunable broadside coupled split ring resonators," *IEEE Microw. Wirel. Components Lett.*, Vol. 23, No. 4, 187–189, 2013.
10. Pourghorban Saghati, A., J. S. Batra, J. Kameoka, and K. Entesari, "A miniaturized microfluidically reconfigurable coplanar waveguide bandpass filter with maximum power handling of 10 Watts," *IEEE Trans. Microw. Theory Tech.*, Vol. 63, No. 8, 2515–2525, 2015.
11. McClung, S. N., S. Saeedi, and H. H. Sigmarsson, "Band-reconfigurable filter with liquid metal actuation," *IEEE Trans. Microw. Theory Tech.*, Vol. 66, No. 6, 3073–3080, 2018.
12. Park, E. and S. Lim, "Microfluidic dual-band bandpass filter," *2017 IEEE Asia Pacific Microwave Conference (APMC)*, 762–764, 2017.
13. Kaur, T. K., L. Osorio, J. L. Olvera Cervantes, J. R. Reyes-Ayona, and A. Corona-Chavez, "Microfluidic reconfigurable filter based on ring resonators," *Progress In Electromagnetics Research Letters*, Vol. 79, 59–63, 2018.
14. Zhou, W. J. and J. X. Chen, "Novel microfluidically tunable bandpass filter with precisely-controlled passband frequency," *Electron. Lett.*, Vol. 52, No. 14, 1235–1236, 2016.
15. Zhou, W. J., H. Tang, and J. X. Chen, "Novel microfluidically tunable differential dual-mode patch filter," *IEEE Microw. Wirel. Components Lett.*, Vol. 27, No. 5, 461–463, 2017.
16. Arbelaez-Nieto, A., E. Cruz-Perez, J. L. Olvera-Cervantes, A. Corona-Chavez, and H. Lobato-Morales, "The perfect balanced — A design procedure for balanced bandpass filters [Applications Notes]," *IEEE Microwave Magazine*, Vol. 16, No. 10, 54–65, Nov. 2015.
17. Arbelaez-Nieto, A., J. L. Olvera-Cervantes, C. E. Saavedra, and A. Corona-Chavez, "Balanced liquid metal reconfigurable microstrip filter," *Journal of Electromagnetic Waves and Applications*, Vol. 31, No. 14, 1453–1466, 2017.
18. Pozar, D. M., *Microwave Engineering*, 4th Edition, Vol. I, John Wiley & Sons, Inc., New York, 2012.
19. Hong, J.-S. and M. J. Lancaster, *Microstrip Filters for RF/Microwave Applications*, John Wiley & Sons, Inc., New York, 2001.
20. Wu, C. H., C. H. Wang, and C. H. Chen, "Novel balanced coupled-line bandpass filters with common-mode noise suppression," *IEEE Trans. Microw. Theory Tech.*, Vol. 55, No. 2, 287–294, 2007.
21. Struck, C. J., "Group delay," *Comput. Sci. Commun. Dict.*, 697–697, 2000.